IEEE Access
Multidisciplinary | Rapid Review | Open Access Journal

Date of publication xxxx 00, 0000, date of current version xxxx 00, 0000.

Digital Object Identifier 10.1109/ACCESS.2017.Doi Number

Thermal Analysis of the Pulse Inductor for Electromagnetic Launch under Continuous Discharge Condition

Fuqiang Ma[1], Baoming Li[1,2]*

[1]National Key Laboratory of Transient Physics, Nanjing University of Science and Technology, Nanjing 210094, Jiangsu, China
[2]China Academy of Ordnance, 100089, Beijing, China

Corresponding author: Baoming Li (e-mail: baomingli@njust.edu.cn).

ABSTRACT The solenoid pulse inductor is a key component of the electromagnetic launch (EML) system, and effective thermal management is a necessary condition for reliable and stable operation under continuous discharge condition. A 3D transient coupling heat transfer model for the solenoid pulse inductor with liquid cooling mode was established, and the temperature distribution and the characteristics of heat dissipation of the inductor under continuous discharge condition has been analyzed. A temperature measurement system was designed, and the accuracy of the 3D coupling model has been verified. In addition, effects of the flow rate, the inlet temperature and the coolant on the efficiency of liquid cooling were analyzed by using this model. The results show that during continuous discharge, the maximum temperature and maximum temperature difference of the inductor continue to increase, but the rising speed rapidly slows down. Raising the flow rate can effectively improve the efficiency of the liquid cooling and decrease the temperature difference in the inductor during continuous discharge, but the marginal benefit of raising the flow rate is gradually reduced. Dropping the inlet temperature has little effect on the efficiency of the liquid cooling, and ethylene glycol solution can replace deionized water as the liquid cooling coolant for the pulse inductor under low temperature condition. This paper is expected to help to improve the thermal management and optimize the performance of the solenoid pulse inductor.

INDEX TERMS continuous discharge, electromagnetic launch (EML), numerical analysis, pulse inductor, thermal analysis

I. INTRODUCTION

The electromagnetic launch (EML) technology accelerates the object to ultra-high speed with the help of electromagnetic thrust, and converts electromagnetic energy into kinetic energy during a very short time to complete various launch tasks. It has the characteristics of short acceleration time, strong muzzle kinetic energy and flexible operation radius, which is favored by military equipment researchers [1-4]. The power required for EML is provided by the high-power pulse power supply (PPS). The capacitive PPS is widely used in EML research due to its mature technology and good reliability [5-6]. As an important component of capacitive PPS, the pulse inductor plays an essential role in adjusting the peak value, the pulse width and variation rate of the discharge current [7-9]. The discharge current of the pulse power supply can reach hundreds of kiloampere, which results in a large amount of heat generated in the pulse inductor. The pulse inductor is generally epoxy resin packaging structure, which is not conducive to heat dissipation. With the development of EML technology, whether continuous pulse discharge can be realized is an important criterion to measure the performance of the PPS [10]. However, continuous pulse discharge will cause heat to accumulate in the pulse inductor, causing a considerable temperature rise. If the pulse inductor cannot be cooled effectively, the energy conversion efficiency of the PPS will decrease, and even lead to thermal damage of the pulse inductor [11]. Therefore, effective thermal management measure is the prerequisite for reliable and stable operation of the pulse inductor under continuous discharge condition. Accurate calculation of the temperature distribution of the pulse inductor is the basis of thermal management system design. Finite element method is widely used in the thermal analysis of the pulse inductor because of its high accuracy.

This article has been accepted for publication in a future issue of this journal, but has not been fully edited. Content may change prior to final publication. Citation information: DOI 10.1109/ACCESS.2021.3089485, IEEE Access

Liu [10] studied the temperature field and thermal stress distribution of coaxial cylinder pulse inductor under single discharge condition by establishing 2D finite element analysis model, and designed relative experiment to verify the calculation results. Yu [11] investigated the thermal accumulation and diffusion process of coaxial cylinder pulse inductor with natural cooling mode by developing the 3D transient heat transfer model, and built a pulse inductor experimental rig to validate the model. Li [12] established a 3D fluid-solid coupling heat dissipation model for the saturated reactor, and researched the effect of thermal conductivity of epoxy resin on heat dissipation performance of saturated reactor. Tong [13] presented a pulse inductor with a circular multi-winding structure with epoxy resin-casting technique, and studied its electromagnetic force, temperature distribution and fatigue behavior by building 3D finite element analysis model. The pulse inductor with solenoid-structure has the advantage of easy cooling design and is more suitable for continuous discharge condition. However, there are few studies on the thermal analysis of solenoid pulse inductor under continuous discharge condition.

The main aim of this paper is to investigate the temperature distribution and the characteristics of heat dissipation of the solenoid pulse inductor with liquid cooling mode under continuous discharge condition. In Section II, a single discharge cycle is divided into discharge stage and discharge interval stage. A 3D electromagnetic-thermal coupling model is established during discharge stage, and a 3D fluid-solid coupling model is established during discharge interval stage. By using this model, the temperature distribution and the characteristics of heat dissipation of the solenoid pulse inductor under continuous discharge condition are analyzed in Section III. To validate the models, a temperature measurement system is designed in Section IV. In order to determine the relative impact of each parameter on the efficiency of liquid cooling, the parameter analysis is performed in Section V. Finally, a summary is given in Section VI. This paper is expected to help to improve the thermal management and optimize the performance of the solenoid pulse inductor.

II. MATHEMATICAL MODEL

In this section, the 3-D transient coupling heat transfer model of the solenoid pulse inductor is established based on theories of electromagnetics, heat transfer and hydrodynamics. The prototype of the solenoid pulse inductor is shown in Fig. 1(a), and Fig. 1(b) shows the installation diagram of the inductor. The coil is wound by a copper tube with a rectangular cross section, and the epoxy resin-casting technique is adopted to reinforce the structure and insulation properties [13]. Deionized water is passed through the copper tube to remove the heat generated during the discharge process. The specific parameters of the solenoid pulse inductor are shown in Table I.

TABLE I
PARAMETERS OF THE SOLENOID PULSE INDUCTOR

Parameters	Value
Height of the inductor(mm)	360
External diameter of the inductor(mm)	195
Internal diameter of inductor(mm)	131
Number of coil turns	23.5
Section size of coil(mm)	12×10
Section size of flow channel(mm)	8×6
Inductance(μH)	28

(a) The prototype of the solenoid pulse inductor

(b) The installation diagram of the solenoid pulse inductor

FIGURE 1. The prototype and installation diagram of the solenoid pulse inductor.

The analysis model of the inductor is shown in Fig. 2. To reduce the complexity of the analysis model, the connection structure between the nozzle and the coil is ignored.

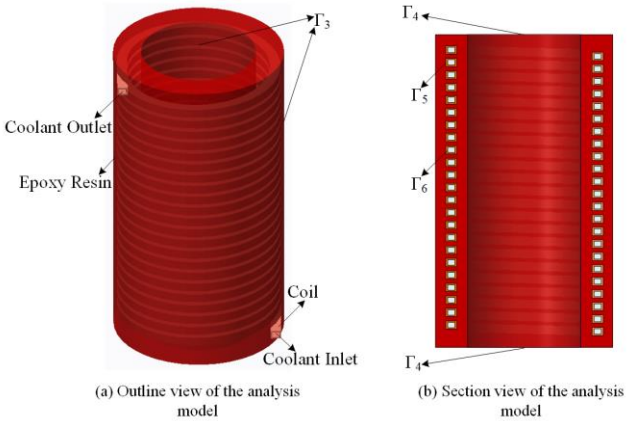

(a) Outline view of the analysis model

(b) Section view of the analysis model

FIGURE 2. The analysis model of the solenoid pulse inductor.

In order to investigate the temperature distribution of the solenoid pulse inductor with liquid cooling mode, the following assumptions have been made.

This article has been accepted for publication in a future issue of this journal, but has not been fully edited. Content may change prior to final publication. Citation information: DOI 10.1109/ACCESS.2021.3089485, IEEE Access

1) The physical parameters of coil and epoxy resin are homogeneous and are not affected by the temperature.
2) The initial temperature of the inductor is uniform and is equal to the ambient temperature.
3) The epoxy resin is ideal insulator, so the influence of epoxy resin can be ignored in the electromagnetic calculation.
4) As the thermal time constant of the coil is far greater than the pulse width of discharge current [14-15], the heat transfer between the coil and the deionized water can be ignored during discharge stage.

Based on the above assumptions, a single discharge cycle is divided into discharge stage and discharge interval stage, and the mathematical model is established respectively, as shown in Fig. 3.

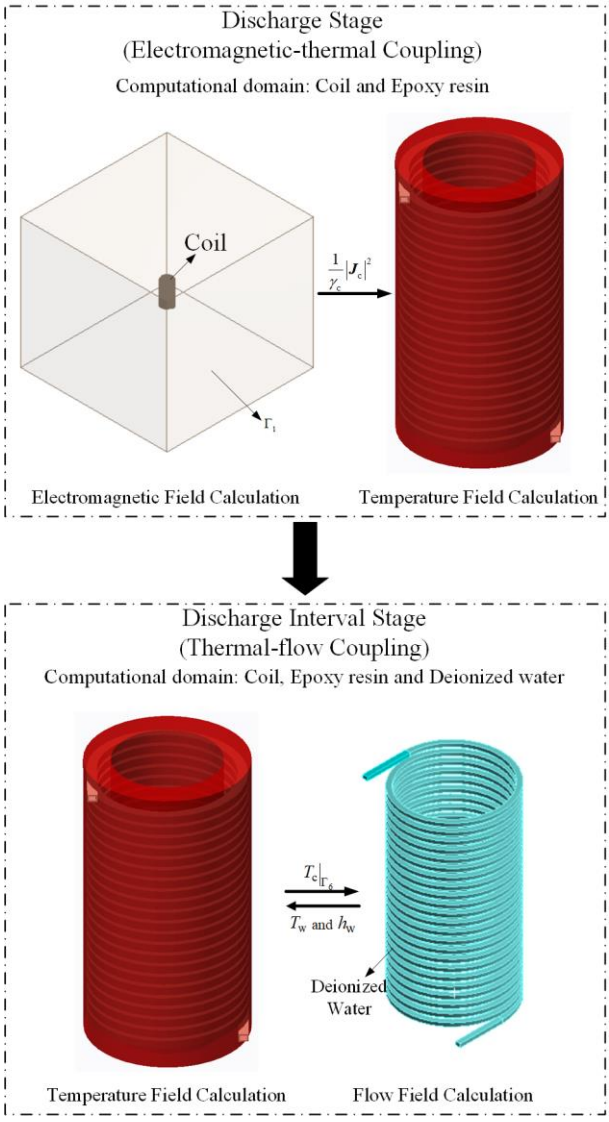

FIGURE 3. The calculation process of a single discharge cycle.

A. DISCHARGE STAGE

During the discharge stage, the mathematical model is electromagnetic-thermal coupling model. The computational domain includes the coil and the epoxy resin. The measured pulsed discharge current and its spectrum distribution are shown in Fig. 4. As the frequency of the discharge current is relatively low, the time-varying electromagnetic field calculation can be simplified to magnetoquasistatic field calculation [16]. The equation for the temperature field calculation is the unsteady heat conduction equation with internal heat source (Joule heating effect) [17]. The mathematical model during the discharge stage is as follows [16-17]

$$\nabla \times \boldsymbol{E}_{\mathrm{c}} = -\frac{\partial \boldsymbol{B}_{\mathrm{c}}}{\partial t} \tag{1}$$

$$\nabla \times \boldsymbol{H}_{\mathrm{c}} = \boldsymbol{J}_{\mathrm{c}} \tag{2}$$

$$\nabla \cdot \boldsymbol{B}_{\mathrm{c}} = 0 \tag{3}$$

$$\boldsymbol{B}_{\mathrm{c}} = \mu_{\mathrm{c}} \boldsymbol{H}_{\mathrm{c}} \tag{4}$$

$$\boldsymbol{J}_{\mathrm{c}} = \gamma_{\mathrm{c}} \boldsymbol{E}_{\mathrm{c}} \tag{5}$$

$$\rho_{\mathrm{c,r}} c_{\mathrm{c,r}} \frac{\partial T_{\mathrm{c,r}}}{\partial t} = \nabla \cdot \left(\kappa_{\mathrm{c,r}} \nabla T_{\mathrm{c,r}} \right) + \frac{1}{\gamma_{\mathrm{c}}} \left| \boldsymbol{J}_{\mathrm{c}} \right|^2 \tag{6}$$

Where, $\boldsymbol{H}$ is magnetic field intensity, $\boldsymbol{J}$ is current density, $\boldsymbol{E}$ is electric intensity, $\boldsymbol{B}$ is magnetic flux density, μ is permeability, γ is conductivity, ρ is density, c is specific heat, κ is thermal conductivity, t is time, T is temperature. The subscript c represents the coil, and the subscript r represents the epoxy resin.

B. DISCHARGE INTERVAL STAGE

During the discharge interval stage, the mathematical model is fluid-solid coupling model. The computational domain includes the coil, the epoxy resin and deionized water. The equation for the temperature field calculation is the unsteady heat conduction equation without internal heat source. The equations for flow field calculation are composed of continuity equation, momentum conservation equation and energy conservation equation [18]. The mathematical model during the discharge interval stage is as follows [17-18]

$$\rho_{\mathrm{c,r}} c_{\mathrm{c,r}} \frac{\partial \boldsymbol{T}_{\mathrm{c,r}}}{\partial t} = \nabla \cdot \left(\kappa_{\mathrm{c,r}} \nabla T_{\mathrm{c,r}} \right) \tag{7}$$

$$\nabla \cdot \boldsymbol{U}_{\mathrm{w}} = 0 \tag{8}$$

$$\frac{\partial (\rho_{\mathrm{w}} \boldsymbol{U}_{\mathrm{w}})}{\partial t} + \nabla \cdot (\rho_{\mathrm{w}} \boldsymbol{U}_{\mathrm{w}} \otimes \boldsymbol{U}_{\mathrm{w}}) = \nabla \cdot ((\nu_{\mathrm{w}} \nabla \otimes \boldsymbol{U}_{\mathrm{w}})^T - p_{\mathrm{w}} \boldsymbol{I}) \tag{9}$$

$$\frac{\partial \left(\rho_{\mathrm{w}} c_{\mathrm{w}} T_{\mathrm{w}} \right)}{\partial t} + \nabla \cdot (\rho_{\mathrm{w}} c_{\mathrm{w}} \boldsymbol{U}_{\mathrm{w}} T_{\mathrm{w}}) = \nabla \cdot \left(\kappa_{\mathrm{w}} \nabla T_{\mathrm{w}} \right) \tag{10}$$

Where, $\boldsymbol{U}$ is velocity, ν is viscosity, p is pressure, $\boldsymbol{I}$ is identity matrix, the subscript w represents deionized water.

This article has been accepted for publication in a future issue of this journal, but has not been fully edited. Content may change prior to final publication. Citation information: DOI 10.1109/ACCESS.2021.3089485, IEEE Access

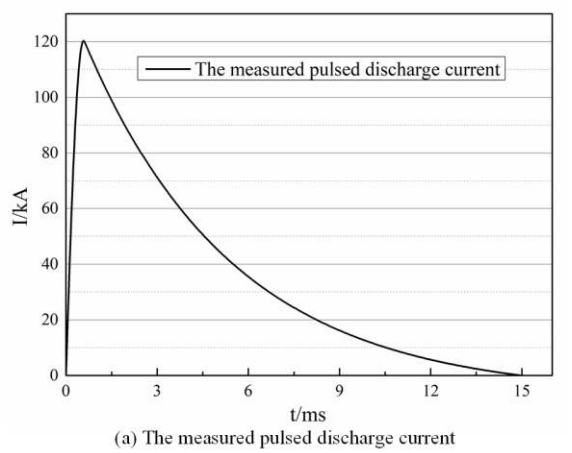

(a) The measured pulsed discharge current

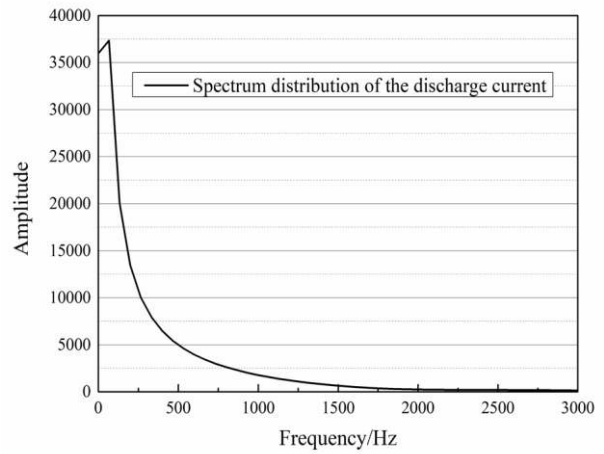

(b) The spectrum distribution of the discharge current

FIGURE 4. The measured pulse discharge current and its spectrum distribution.

C. BOUNDARY CONDITIONS

At the boundary of the electromagnetic field calculation domain (Γ_1), $\boldsymbol{B}$ and $\boldsymbol{E}$ obey natural boundary condition. The boundary conditions are as follows:

$$\boldsymbol{B}_{\mathrm{c}}\big|_{\Gamma_1}=0,\boldsymbol{E}_{\mathrm{c}}\big|_{\Gamma_1}=0 \tag{11}$$

$\boldsymbol{E}$ and $\boldsymbol{H}$ is continuous in the tangential direction of the surface of the coil (Γ_2), $\boldsymbol{B}$ is continuous in the normal direction of Γ_2. The boundary conditions are as follows:

$$\begin{aligned}\boldsymbol{e}_{\mathrm{n}}\times(\boldsymbol{E}_{\mathrm{c}}\big|_{\Gamma_2^+}-\boldsymbol{E}_{\mathrm{c}}\big|_{\Gamma_2^-})=0\\ \boldsymbol{e}_{\mathrm{n}}\times(\boldsymbol{H}_{\mathrm{c}}\big|_{\Gamma_2^+}-\boldsymbol{H}_{\mathrm{c}}\big|_{\Gamma_2^-})=0\\ \boldsymbol{e}_{\mathrm{n}}\cdot(\boldsymbol{B}_{\mathrm{c}}\big|_{\Gamma_2^+}-\boldsymbol{B}_{\mathrm{c}}\big|_{\Gamma_2^-})=0\end{aligned} \tag{12}$$

Where, $\boldsymbol{e}_{\mathrm{n}}$ is the normal direction of the boundary.

At the lateral surface of the inductor (Γ_3), the boundary is air natural convection heat transfer boundary. The boundary condition is as follows:

$$-\kappa_{\mathrm{r}}\left(\frac{\partial T_{\mathrm{r}}}{\partial \boldsymbol{e}_{\mathrm{n}}}\right)\Big|_{\Gamma_3}=h_{\mathrm{am}}\left(T_{\mathrm{r}}\big|_{\Gamma_3}-T_{\mathrm{am}}\right) \tag{13}$$

Where, h_{am} is the heat transfer coefficient of air natural convection, the subscript am represents the ambient. As the heat transfer coefficient of air natural convection is generally between 1 W/(m^2·K) and 10 W/(m^2·K) [17], h_{am} is set as 10 W/(m^2·K) in this paper.

As shown in Fig. 1(b), the top and bottom surface of the inductor (Γ_4) are covered by insulation plates. Considering the poor thermal conductivity of the insulation plates and the contact thermal resistance, heat transfer between the inductor and insulation plates can be ignored. So the top and bottom surface of the inductor (Γ_4) is regarded as adiabatic boundary. The boundary condition is as follows:

$$-\kappa_{\mathrm{r}}\left(\frac{\partial T_{\mathrm{r}}}{\partial \boldsymbol{e}_{\mathrm{n}}}\right)\Big|_{\Gamma_4}=0 \tag{14}$$

The thermal contact between the coil and the epoxy resin is non-ideal thermal contact. So at the contact face between the coil and the epoxy resin (Γ_5), the boundary conditions are as follows:

$$\begin{aligned}T_{\mathrm{c}}\big|_{\Gamma_5}=T_{\mathrm{r}}\big|_{\Gamma_5}+\boldsymbol{q}\big|_{\Gamma_5}\cdot R_{\mathrm{ctr}}\\ \boldsymbol{q}\big|_{\Gamma_5}=-\kappa_{\mathrm{c}}\frac{\partial T_{\mathrm{c}}}{\partial \boldsymbol{e}_{\mathrm{n}}}\Big|_{\Gamma_5}=-\kappa_{\mathrm{r}}\frac{\partial T_{\mathrm{r}}}{\partial \boldsymbol{e}_{\mathrm{n}}}\Big|_{\Gamma_5}\end{aligned} \tag{15}$$

Where, $\boldsymbol{q}$ is heat flux, $\boldsymbol{R}_{\mathrm{ctr}}$ is contact thermal resistance between the coil and epoxy resin. According to the factory report, the value of $\boldsymbol{R}_{\mathrm{ctr}}$ is 0.0008(m^2·K)/W.

At the contact face between the coil and deionized water (Γ_6), the boundary is forced convection heat transfer boundary and no-slip boundary. The boundary conditions are as follows:

$$\begin{aligned}\boldsymbol{U}_{\mathrm{w}}\big|_{\Gamma_6}=0\\ h_{\mathrm{w}}=\frac{-\kappa_{\mathrm{w}}\dfrac{\partial T_{\mathrm{w}}}{\partial \boldsymbol{e}_{\mathrm{n}}}\Big|_{\Gamma_6}}{T_{\mathrm{w}}\big|_{\Gamma_6}-\overline{T_{\mathrm{w}}}}\\ -\kappa_{\mathrm{c}}\left(\frac{\partial T_{\mathrm{c}}}{\partial \boldsymbol{e}_{\mathrm{n}}}\right)\Big|_{\Gamma_6}=h_{\mathrm{w}}\left(T_{\mathrm{c}}\big|_{\Gamma_6}-T_{\mathrm{w}}\right)\end{aligned} \tag{16}$$

Where, h_{w} is the force convective heat transfer coefficient between the inductor and deionized water.

The initial conditions are as follows:

$$\begin{aligned}\boldsymbol{B}_{\mathrm{c}}=0\\ \boldsymbol{E}_{\mathrm{c}}=0\\ T_{\mathrm{c,r}}=T_{am}\end{aligned} \tag{17}$$

III. THERMAL ANALYSIS

According to the research needs of the current EML system, the pulse inductor needs to withstand more than10 discharges at the frequency of 10 times/min. The maximum

This article has been accepted for publication in a future issue of this journal, but has not been fully edited. Content may change prior to final publication. Citation information: DOI 10.1109/ACCESS.2021.3089485, IEEE Access

allowable temperature of epoxy resin for the pulse inductor is 403.15K under long term operation condition [19]. Considering the safety margin, the maximum temperature of the solenoid pulse inductor needs to be below 393.15K during continuous discharges.

Physical parameters of the coil and epoxy resin are shown in Table II, physical parameters of deionized water are fitted as function of temperature, the general formula is shown in (18), and the coefficient is shown in Table III.

$$\varphi_1 = a_1 + a_2 T + a_3 T^2 + a_4 T^3 + a_5 T^4 \quad (18)$$

Where, the temperature range is 273.15K-373.15K.

TABLE II
PHYSICAL PARAMETERS OF COPPER AND EPOXY RESIN

Parameter	Copper	Epoxy Resin
γ/(S/m)	5.8×10^{7}	-
μ(T·m/A)	1.257×10^{-6}	-
ρ/(kg/m^3)	8933	2200
c/(J/kg·K)	385	503
κ/(W/(m·K))	400	0.26

TABLE III
PHYSICAL PARAMETER COEFFICIENT OF DEIONIZED WATER

φ_1	ρ/(kg/m^3)	c/(J/kg·K)	κ/(W/(m·K))	υ/(kg/m·s)
a_1	816.7876	7212.2	-2.4025	2.2061
a_2	1.48	-23.6206	2.1758×10^{-2}	-2.3535×10^{-3}
a_3	-2.9442×10^{-3}	5.8249×10^{-2}	-5.0848×10^{-5}	9.4569×10^{-6}
a_4	-	-4.4064×10^{-5}	3.9387×10^{-8}	-1.6916×10^{-8}
a_5	-	-	-	1.1350×10^{-11}

Based on the coupling model built in Section II, the temperature distribution of the solenoid pulse under continuous discharge is analyzed by finite element method. The frequency of pulse discharge is 10tmes/min, and the pulse number is 10. The initial temperature of the inductor is equal to the ambient temperature, 298.15K. The flow rate of deionized water is 5L/min, and the inlet temperature of deionized water is 298.15K.

The simulation results are shown in the Fig. 5 and Fig. 6. Fig. 5 shows the temperature distribution at middle section plane of the inductor during continuous discharge. It can be observed that, during continuous discharge, the temperature of the inductor in the outlet zone is the highest and continues to increase; however, the temperature of the inductor in the inlet zone is the lowest and does not change much. That is because the deionized water is heated during the flow process, and the cooling power gradually decreases from the inlet to the outlet. This causes the temperature difference in the inductor to increase with continuous discharge. As shown in partial enlarged drawing, there is an obvious temperature gradient on the contact surface between the coil and epoxy resin, which is because of non-ideal thermal contact. Due to the skin effect and the proximity effect of the discharge current [9], the temperature distribution in cross section of the coil is not uniform.

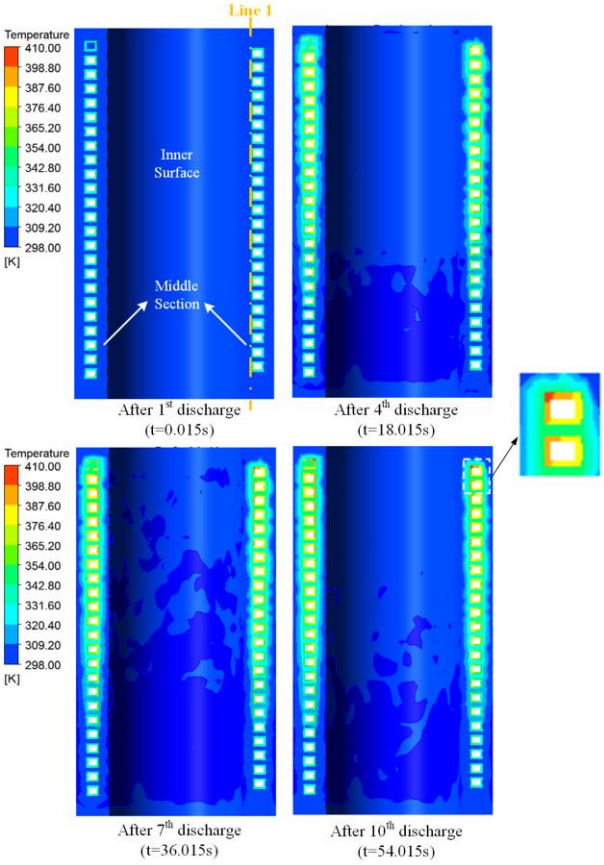

FIGURE 5. Temperature distribution at middle section of the inductor

Fig. 6(a) shows the variation of the maximum temperature of the inductor during continuous discharge. It can be observed that the maximum temperature of the coil and the epoxy resin increases with continuous discharge, but the rising speed rapidly slows down. The maximum temperature of the inductor after the 10th discharge is 407.04K, and is only 0.18K higher than that after the 9th discharge, which means the heat accumulated in the inductor basically no longer increases after 9th discharge cycle. As shown in partial enlarged drawing, the variation of the maximum temperature of the epoxy resin lags behind that of the coil, due to the influence of contact thermal resistance, which is helpful to prevent the epoxy resin from thermal damage. Most of the time, the outlet temperature of the deionized water is equal to the maximum temperature of the inductor, which means the maximum temperature of the inductor can be monitored by measuring the outlet temperature of the deionized water.

Fig. 6(b) shows the variation of heat transfer during continuous discharge. It can be observed that the forced convection heat transfer between the deionized water and the coil is the main way of heat dissipation, and the contribution of air natural convection heat transfer can be neglected. The heat transfer between the coil and the epoxy resin is small, thus most of the accumulated heat of the inductor is stored in the coil. As the maximum temperature of the inductor after 10th discharge exceeds the allowable temperature, the liquid cooling conditions with inlet temperature of 298.15K and

This article has been accepted for publication in a future issue of this journal, but has not been fully edited. Content may change prior to final publication. Citation information: DOI 10.1109/ACCESS.2021.3089485, IEEE Access

flow rate of 5L/min cannot meet the temperature control requirements of the inductor during continuous discharge.

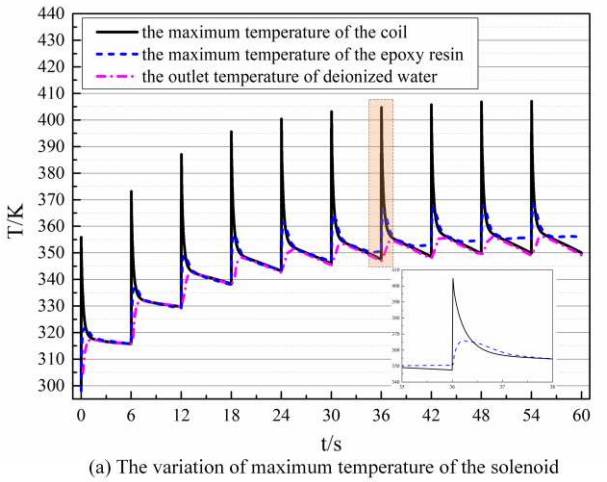

(a) The variation of maximum temperature of the solenoid pulse inductor during 10 discharges

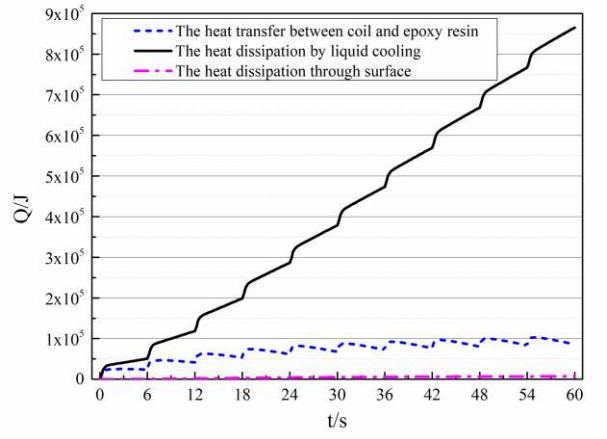

(b) The variation of heat transfer during 10 discharges

FIGURE 6. Thermal analysis results of the solenoid inductor during 10 discharges.

IV. MODEL VALIDATION

Due to the epoxy resin packaging structure, the internal temperature of the solenoid pulse inductor cannot be measured directly. And due to the low thermal diffusivity of the epoxy resin, the surface temperature of the inductor does not change much during continuous discharge. So the outlet temperature during continuous discharge and the surface temperature of the inductor at 120s after continuous discharge are chosen to validate the analysis model.

The measurement system is shown in Fig. 7. Fig. 7(a) shows the schematic diagram of the measurement system. Due to the advantages of low thermal inertia and high accuracy [20], the K-type thermocouples are selected as temperature sensor, and include 2 K-type sheathed thermocouples and 6 K-type thin-film thermocouples. The location of these thermocouples is shown in Fig. 7(b). The data acquisition card is made by the USB_DAQ module of Hengkai Technology. A Labview routine was developed to control the measurement system. The accuracy of the measurement system is 0.2K, and the response time of the measurement system is 0.1s.

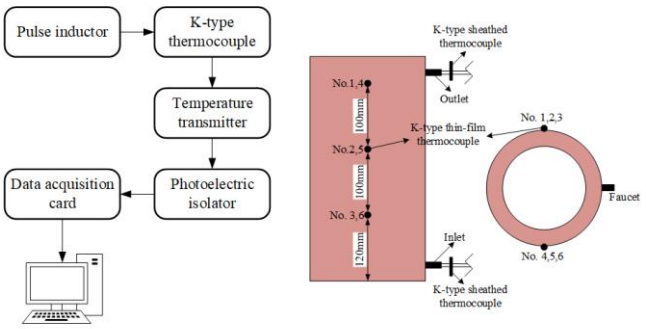

(a) The schematic diagram of the measurement system

(b) The location of the thermocouple

FIGURE 7. The measurement system

The experiment of 10 discharges was carried at the frequency of 10 times/min. The experiment parameters are shown in Table IV. The flow rate of the deionized water is 7L/min and the inlet temperature of the deionized water is 295.8K.

TABLE IV
EXPERIMENT PARAMETERS

Parameter	Value
Discharge voltage	10kV
Pulse width	15ms
Discharge number	10
Discharge interval	6s
Discharge duration	54s
Ambient temperature	295.8K
Initial temperature of the inductor	295.8K

The comparison of the simulation results and experimental results is shown in Fig. 8. Fig. 8(a) shows the comparison of outlet temperature of deionized water during continuous discharge, and Fig. 8(b) shows the comparison of the temperature of measuring point at 120s after 10^{th} discharge. It can be observed that the experiment results are slightly larger than the simulation results. The reasons for the deviation may be as follows:

1) The effect of temperature on the resistance of the coil was ignored in simulation analysis;
2) The response delay of the measurement system affected the experimental results.

For outlet temperature of deionized water, the maximum deviation is 3.3K and the average deviation is 2.34K. For the temperature of measuring points, the maximum deviation is 2.9K and the average deviation is 2.42K. As the difference between the simulation results and the experimental results are small, and the tendency is same, the reliability and accuracy of the 3-D transient coupling heat transfer model of the solenoid pulse inductor have been verified.

This article has been accepted for publication in a future issue of this journal, but has not been fully edited. Content may change prior to final publication. Citation information: DOI 10.1109/ACCESS.2021.3089485, IEEE Access

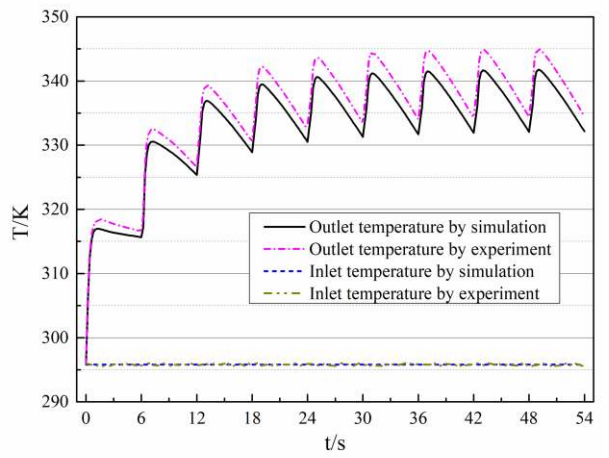

(a) Inlet and outlet temperature of deionized water during continuous discharge

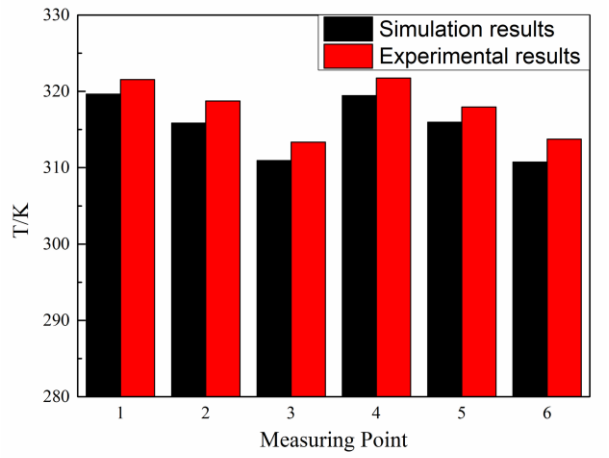

(b) Temperature of measuring point at 120s after 10th discharge

FIGURE 8. Comparison of experimental results and simulation results

V. PARAMETRIC ANALYSIS

The efficiency of the liquid cooling during continuous discharge involves many factors. The parametric analysis provides the information to determine the relative influence of each factor and, thus, to improve the thermal management and optimize its working condition for the solenoid pulse inductor. As the inductance of the solenoid pulse inductor is related to its structure and size [21-22], the structure and size of the flow channel are generally not changed during thermal management design stage. The parameters selected to analyze are the flow rate, the inlet temperature and the coolant.

A. IMPACT ANALYSIS OF THE FLOW RATE

The flow rate is a key factor that affects the convective heat transfer coefficient between the pulse inductor and the coolant. Fig. 9 shows the thermal analysis results of the inductor at flow rate of 5L/min, 7L/min, 9L/min and 11L/min. The coolant is deionized water, and the inlet temperature is 298.15K.

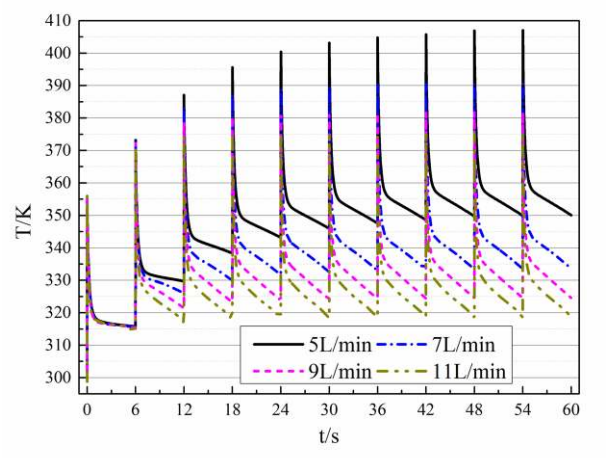

(a) Influence of the flow rate on the maximum temperature of the inductor

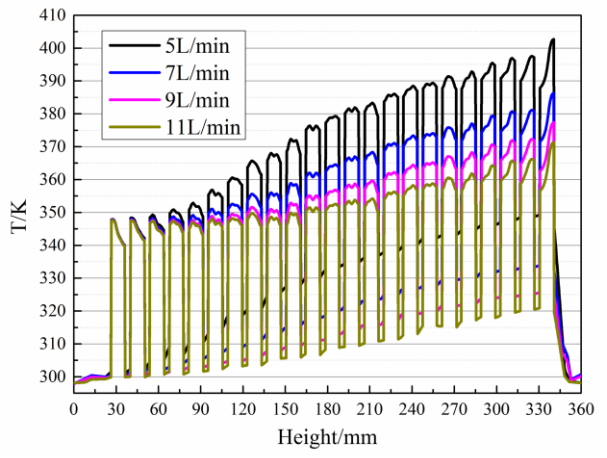

(b) Influence of the flow rate on the temperature distribution of the inductor along Line 1 (shown in Fig. 5) after 10th discharge

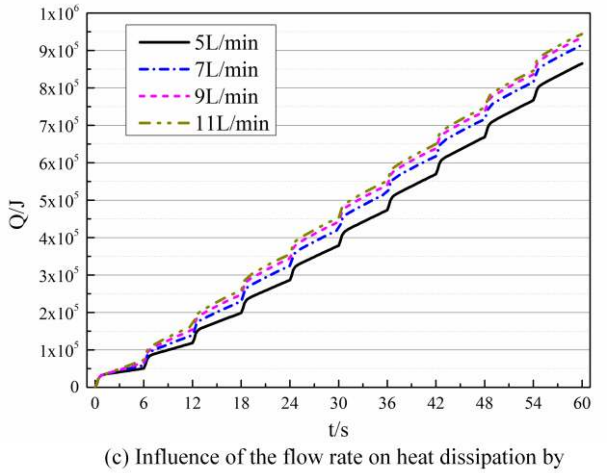

(c) Influence of the flow rate on heat dissipation by liquid cooling

FIGURE 9. Influence of the flow rate on thermal analysis results of the inductor.

Fig. 9(a) shows the effects of the flow rate on the maximum temperature of the inductor. It can be observed that the maximum temperature of the inductor decreases

This article has been accepted for publication in a future issue of this journal, but has not been fully edited. Content may change prior to final publication. Citation information: DOI 10.1109/ACCESS.2021.3089485, IEEE Access

rapidly with the rise of the flow rate. After the 10th discharge (54.015s), the maximum temperature of the inductor has decreased by 16.3K, 25.3K and 31.4K with the rise in flow rate from 5L/min to 7L/min, 9L/min and 11L/min, respectively, and the maximum temperature difference in the inductor decreased by 16.1K, 25.1K and 31.3K, as shown in Fig. 9(b). Fig. 9(c) shows the effects of the flow rate on the heat dissipation by liquid cooling, and after the 10th discharge cycle (60s), the dissipation by liquid cooling has increased by 49.3kJ, 69.2kJ and 78.3kJ with the rise in flow rate from 5L/min to 7L/min, 9L/min and 11L/min, respectively.

This indicates that raising the flow rate can effectively improve the efficiency of the liquid cooling and decrease the temperature difference in the inductor during continuous discharge, but the marginal benefit of raising the flow rate is gradually reduced. When the coolant is deionized water and the inlet temperature is 298.15K, the temperature control requirements of the inductor during continuous discharge can be met as long as the flow rate is greater than 7L/min.

B. IMPACT ANALYSIS OF THE INLET TEMPERATURE

The inlet temperature is a factor that affects the temperature difference between the inductor and the coolant. Fig. 10 shows the thermal analysis results of the inductor at inlet temperature of 298.15K, 293.15K and 288.15K. The coolant is deionized water, and the flow rate is 5L/min.

Fig. 10(a) shows the effects of the inlet temperature on the maximum temperature of the inductor. It can be observed that the maximum temperature of the inductor decreases slightly with the drop of the inlet temperature. After the 10th discharge (54.015s), the maximum temperature of the inductor has decreased by 5.5K and 10.2K with the drop in inlet temperature from 298.15K to 293.15K and 288.15K, respectively, and the maximum temperature difference in the inductor decreased by 3.5K and 4.1K, as shown in Fig. 10(b). Fig. 10(c) shows the effects of the inlet temperature on the heat dissipation by liquid cooling, and after the 10th discharge cycle (60s), the dissipation by liquid cooling has increased by 29.1kJ and 55.2kJ with the drop in inlet temperature from 298.15K to 293.15K and 288.15K, respectively.

This indicates that dropping the inlet temperature has little effect on the efficiency of the liquid cooling and the temperature difference in the inductor during continuous discharge. As the inlet temperature must be more than 2K higher than the local dew point [23], during the thermal management design stage, the inlet temperature of the coolant should be equal to the ambient temperature.

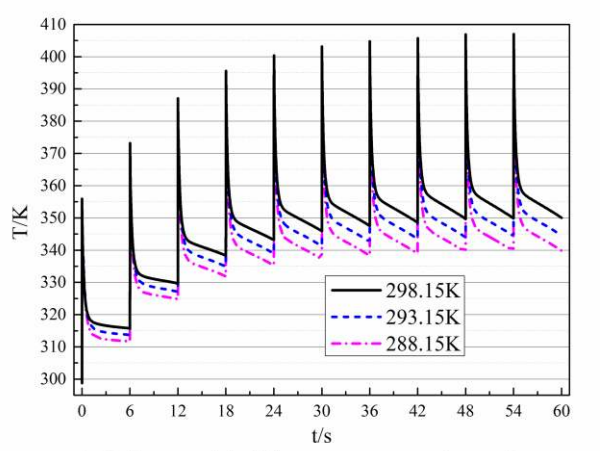

(a) Influence of the inlet temperature on the maximum temperature of the inductor

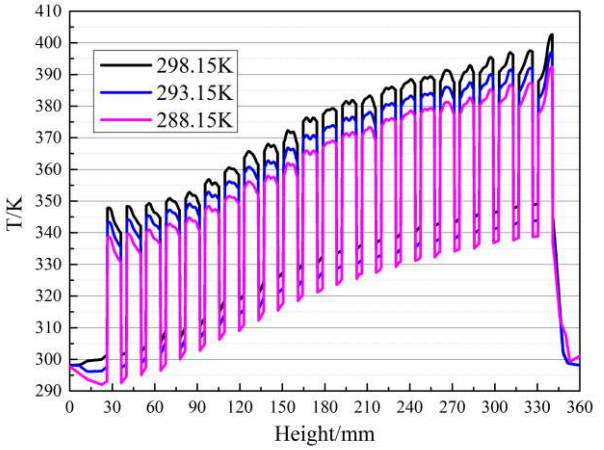

(b) Influence of the inlet temperature on the temperature distribution of the inductor along Line 1 (shown in Fig. 5) after 10th discharge

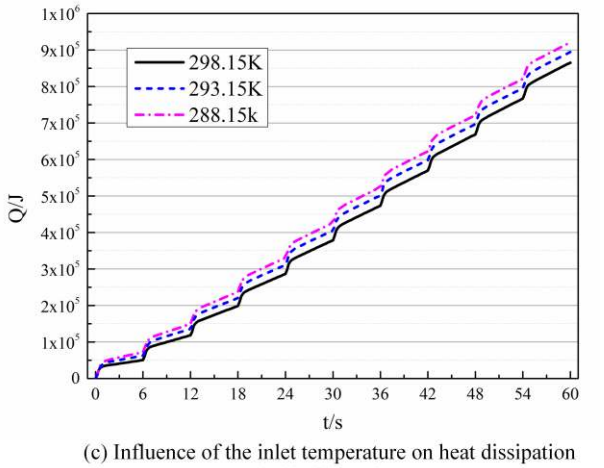

(c) Influence of the inlet temperature on heat dissipation by liquid cooling

FIGURE 10. Influence of the inlet temperature on thermal analysis results of the inductor.

This article has been accepted for publication in a future issue of this journal, but has not been fully edited. Content may change prior to final publication. Citation information: DOI 10.1109/ACCESS.2021.3089485, IEEE Access

C. IMPACT ANALYSIS OF THE COOLANT

When the ambient temperature is lower than 273.15k, deionized water cannot be used as coolant because of freezing. This can be solved by adding ethylene glycol to deionized water. Ethylene glycol is colorless transparent viscous liquid, and can be used as aqueous-freezing-point depressant. When the concentration of ethylene glycol by mass is 40%, the freezing point of the solution is 250.85K; and when the concentration of ethylene glycol by mass is 60%, the freezing point of the solution is 224.85K [24]. In addition, the addition of ethylene glycol does not affect the insulation performance of deionized water [25]. Fig. 11 shows the thermal analysis results of the inductor when the coolant is deionized water, aqueous solution of 40% ethylene glycol by mass and aqueous solution of 60% ethylene glycol by mass. The flow rate is 7L/min, and the inlet temperature is 298.15K. The physical parameters of the ethylene glycol aqueous solution are shown in Table V [24]. As temperature has little effect on the density, specific heat and thermal conductivity of the solution, the effects of temperature on the density, specific heat and thermal conductivity of the solution are ignored, and only the effects of temperature on the viscosity of the solution are considered.

TABLE V
PHYSICAL PARAMETERS OF ETHYLENE GLYCOL AQUEOUS SOLUTION

Mass Fraction	ρ (kg/m^3)	c (J/kg·K)	κ (W/(m·K))	υ (kg/m·s)
40%	1057.6	3485	0.408	φ_2
60%	1083.87	3106	0.336	φ_3

$$\varphi_2 = 0.219196 - 1.80256\times10^{-3}T + 4.99387\times10^{-6}T^2 - 4.64555\times10^{-9}T^3 \quad (19)$$

$$\varphi_3 = 0.54477 - 4.55361\times10^{-3}T + 1.22726\times10^{-5}T^2 - 1.19992\times10^{-8}T^3 \quad (20)$$

Where, the temperature range is 298.15K-373.15K.

Fig. 11(a) shows the effects of the coolant on the maximum temperature of the inductor. It can be observed that the addition of ethylene glycol will slightly increase the maximum temperature of the inductor during continuous discharge. After the 10th discharge (54.015s), the maximum temperature of the inductor has increased by 5.7K and 10.6K with the mass fraction of ethylene glycol from 0% to 40% and 60%, respectively, and the maximum temperature difference in the inductor increased by 4.6K and 9.4K, as shown in Fig. 11(b). Fig. 11(c) shows the effects of the coolant on the heat dissipation by liquid cooling, and after the 10th discharge cycle (60s), the dissipation by liquid cooling has decreased by 34.3kJ and 52.4kJ with the mass fraction of ethylene glycol from 0% to 40% and 60%, respectively.

This indicates that adding ethylene glycol to deionized water has little effect on the efficiency of the liquid cooling and the temperature difference in the inductor during continuous discharge. Thus, under low temperature conditions, ethylene glycol solution can replace deionized water as the liquid cooling coolant for the pulse inductor under continuous discharge condition.

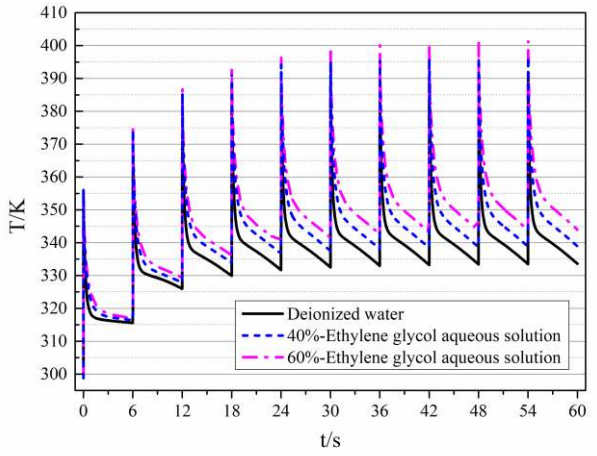

(a) Influence of the coolant on the maximum temperature of the inductor

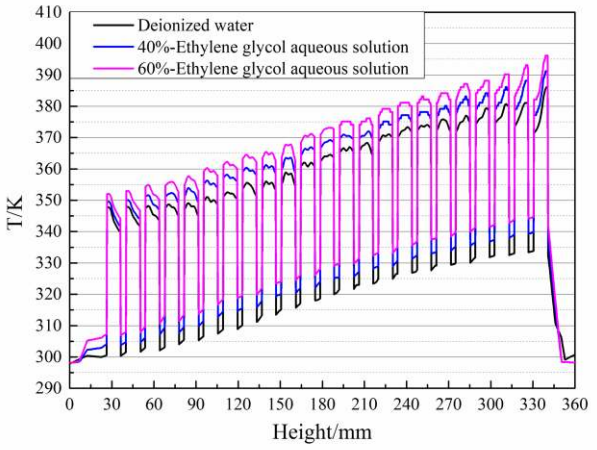

(b) Influence of the coolant on the temperature distribution of the inductor along Line 1 (shown in Fig. 5) after 10th discharge

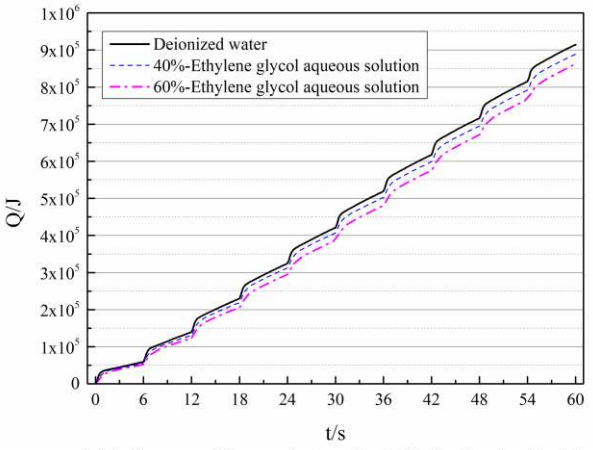

(c) Influence of the coolant on heat dissipation by liquid cooling

FIGURE 11. Influence of the coolant on thermal analysis results of the inductor.

This article has been accepted for publication in a future issue of this journal, but has not been fully edited. Content may change prior to final publication. Citation information: DOI 10.1109/ACCESS.2021.3089485, IEEE Access

VI. CONCLUSIONS

A 3D transient coupling heat transfer model for the solenoid pulse inductor with liquid cooling mode was established, and the temperature distribution and the characteristics of heat dissipation of the inductor under continuous discharge condition has been analyzed. A temperature measurement system was designed to measure the outlet temperature of deionized water during continuous discharge and the surface temperature of the inductor at 120s after continuous discharge, and the accuracy of the 3D coupling model has been verified. Furthermore, effects of the flow rate, the inlet temperature and the coolant on the efficiency of liquid cooling were analyzed by using this model. The results can help to improve the thermal management and optimize the performance of the solenoid pulse inductor. The following conclusions were obtained:

- During continuous discharge, the temperature of the inductor in the outlet zone is the highest and continues to increase, but the rising speed rapidly slows down; the temperature of the inductor in the inlet zone is the lowest and does not change much.
- The maximum temperature difference of the inductor continues to increase, but the rising speed rapidly slow down during continuous discharge.
- Due to the non-ideal thermal contact, there is an obvious temperature gradient between the coil and epoxy resin, and the temperature change of epoxy resin lags behind that of the coil, which is helpful to prevent the epoxy resin from thermal damage.
- The forced convection heat transfer between the deionized water and the coil is the main way of heat dissipation, and most of the accumulated heat during continuous discharge is stored in the coil.
- Raising the flow rate can effectively improve the efficiency of the liquid cooling and decrease the temperature difference in the inductor during continuous discharge, but the marginal benefit of raising the flow rate is gradually reduced.
- Dropping the inlet temperature has little effect on the efficiency of the liquid cooling and the temperature difference in the inductor during continuous discharge. And the inlet temperature should be equal to the ambient temperature when designing the thermal management.
- Under low temperature conditions, ethylene glycol solution can replace deionized water as the liquid cooling coolant for the pulse inductor under continuous discharge condition.

REFERENCES

[1] H. D. Fair, "Progress in Electromagnetic Launch Science and Technology," *IEEE Transactions on Magnetics*, vol. 43, no. 1, pp. 93-98, Jan. 2007.

[2] J. Li, P. Yan and W. Q. Yuan, "Electromagnetic Gun Technology and Its Development," *High Voltage Engineering*, vol. 40, no. 4, pp. 1052-1064, 2014.

[3] B. M. Li and Q. H. Lin, "Analysis and Discussion on Launching Mechanism and Tactical Electromagnetic Railgun Technology," *Defence Technology*, vol. 14, no. 5, pp. 484-495, Oct. 2018.

[4] W. M. Ma, J. Y. Lu and Y. Q. Liu, "Research Progress of Electromagnetic Launch Technology," *IEEE Transactions on Plasma Science*, vol. 47, no. 5, pp. 2197-2205, May. 2019.

[5] R. F. Ramazanov *et al.*, "Conceptual Design of 2 MJ Capacitive Energy Storage," *Defence Technology*, vol. 14, no. 5, pp. 622-627, Oct. 2018.

[6] Z. X. Li *et al.*, "Current Situation and Development of Pulsed Power Supply Module Technology for Electric Gun," *Acta Armamentarii*, vol. 41, no. s1, pp. 1-7, Apr. 2020.

[7] E. Spahn, G. Buderer and W. Wenning, "A Compact Pulse Forming Network, Based on Semiconducting Switches, for Electric Gun Applications," *IEEE Transactions on Magnetics*, vol. 35, no. 1, pp. 378-382, Jan. 1999.

[8] L. Dai *et al.*, "Research on a Miniaturized Pulsed Inductor Applied in PPS," in *16th International Symposium on Electromagnetic Launch Technology*, Beijing, China, 2012, pp. 1-6.

[9] X. H. Yu *et al.*, "Simulation of Electromagnetic Force Between Pulsed Inductor and Internal Structure of Power Supply Module," *IEEE Transactions on Plasma Science*, vol. 41, no. 5, pp. 1237-1242, May. 2013.

[10] J. Liu *et al.*, "Analysis for Temperature Field and Thermal Stress of the Pulsed Inductor," *IEEE Transactions on Plasma Science*, vol. 41, no. 5, pp. 1220-1224, May. 2013.

[11] Y. S. Yu, J. N. Dong and J. Zhang, "Thermal Performance Study on Pulsed Inductor," *IEEE Transactions on Plasma Science*, vol. 43, no. 5, pp. 1185-1189, May 2015.

[12] X. Y. Li *et al.*, "Effect of High-Thermal Conductivity Epoxy Resin on Heat Dissipation Performance of Saturated Reactor," *IEEE Transactions on Dielectrics and Electrical Insulation*, vol. 24, no. 6, pp. 3898-3905, Dec. 2017.

[13] W. Tong *et al.*, "Preliminary Design of Pulse Inductor Applied for 100-kA Quench Protection System," *IEEE Transactions on Plasma Science*, vol. 48, no. 6, pp. 1754-1761, Jun. 2020.

[14] L. J. Wang *et al.*, "Numerical and Experimental Validation of Variation of Power Transformers' Thermal Time Constants with Load Factor," *Applied Thermal Engineering*, vol. 126, pp. 939-948, Nov. 2017.

[15] Muna E. Raypah *et al.*, "Thermal Characterizations Analysis of High-power ThinGaN Cool-white Light-emitting Diodes," *Journal of Applied Physics*, vol. 123, no. 10, pp. 105703, Mar. 2018.

[16] Q. Z. Ye and D. Z. Chen, "Quasi-static field," in *Electromagnetic Field*, Beijing, China: Machine Press, 2019, pp. 241-254.

[17] S. M. Yang and W. Q. Tao, "Unsteady heat conduction," in *Heat Transfer*, 4th ed., Beijing, China: Higher Education Press, 2006, pp. 6-8+115-123.

[18] J. D. Anderson, "Governing equations of fluid dynamics," in *Computational Fluid Dynamics: the Basics with Applications*, Beijing, China: Machine Press, 2007, pp. 51-57.

[19] Z. X. Li *et al.*, "Compact Pulsed Power Module for Electrothermal Chemical Launch" *High Voltage Engineering*, vol. 46, no. 10, pp. 3699-3707, 2020.

[20] X. B. Ye *et al.*, "Temperature measured by thermocouple," in *Sensors and Detective Technique*,

Beijing, China: National Defense Industry Press, 2007, pp. 285-297.

[21] P. P. Biringer, P. P. Burke and R. S. Segsworth, "Inductance of Magnetically Shielded Air-core Coils of Circular Cross Section," *IEEE Transactions on Magnetics*, vol. 5, no. 1, pp. 56-60, Mar. 1969.

[22] C. D. Sijoy and S. Chaturvedi, "Fast and Accurate Inductance Calculations for Arbitrarily-Wound Coils for Pulsed Power Applications," in *15th IEEE International Pulsed Power Conference*, Monterey, CA, USA, 2005, pp. 1464-1467.

[23] L. J. Wang and C. S. Yang, "Research and Application of the Formula for Dew Point Temperature of Moist Air," *Equipment Manufacturing Technology*, no. 5, pp. 124-126+144, 2019.

[24] *ASHRAE handbook: fundamentals*, SI ed., Air-Conditioning Engineers, Atlanta, GA, USA, 2017, pp. 31.4-31.8.

[25] Fenneman, D. B., "Pulsed High-Voltage Dielectric-Properties of Ethylene-Glycol Water Mixtures," *Journal of Applied Physics*, vol. 53, no. 12, pp. 8961-8968, 1982.

FUQIANG MA received the B.S. degree in naval architecture and ocean engineering from the Huazhong University of Science and Technology, China, in 2013. He is currently pursuing the PH.D. with the Nanjing University of Science and Technology. His research interests include electromagnetic launch technology and pulsed power supply technology.

BAOMING LI received the PH. D. from the Nanjing University of Science and Technology, China, in 1992. He is currently a Professor with the Nanjing University of Science and Technology. He has published more than 200 research papers in journals and conference proceedings. He is a director of the international ballistics society and the chairman of the publication committee. His research interests include electromagnetic launch technology and pulsed power supply technology.